

Cross Domain Early Crop Mapping using CropGAN and CNN Classifier

Yiqun WANG, Hui HUANG, Radu STATE

Abstract—Driven by abundant satellite imagery, machine learning-based approaches have recently been promoted to generate high-resolution crop cultivation maps to support many agricultural applications. One of the major challenges faced by these approaches is the limited availability of ground truth labels. In the absence of ground truth, existing work usually adopts the "direct transfer strategy" that trains a classifier using historical labels collected from other regions and then applies the trained model to the target region. Unfortunately, the spectral features of crops exhibit inter-region and inter-annual variability due to changes in soil composition, climate conditions, and crop progress, the resultant models perform poorly on new and unseen regions or years. This paper presents the Crop Generative Adversarial Network (CropGAN) to address the above cross-domain issue. Our approach does not need labels from the target domain. Instead, it learns a mapping function to transform the spectral features of the target domain to the source domain (with labels) while preserving their local structure. The classifier trained by the source domain data can be directly applied to the transformed data to produce high-accuracy early crop maps of the target domain. Comprehensive experiments across various regions and years demonstrate the benefits and effectiveness of the proposed approach. Compared with the widely adopted direct transfer strategy, the F1 score after applying the proposed CropGAN is improved by 13.13% – 50.98%.

Index Terms—Early Crop Mapping, Cross Domain, Domain Adaptation, CropGAN, Cropland Data Layer.

I. INTRODUCTION

EARLY crop mapping, i.e. determining the cultivation regions of crops before their harvest season, is the fundamental building block for agricultural planning, resource allocation, crop insurance, risk management [1], [2] and many other agricultural applications. Since the spectral features of vegetation are determined by their structure, leaf biochemistry and phenological stages [3], time-series analysis on multi-spectral images captured by satellites is the dominant approach for land cover classifications. With the rapid growth in data volume and increasing accessibility of satellite imagery, deep learning (DL) based remote sensing has been promoted in recent years to produce high-resolution, high-accuracy crop cultivation maps [4]. This class of approaches relies on a large amount of ground truth data, also known as labels, to

train and validate the classification model. The ground truth can be obtained from surveys as first-hand labels [5], [6], or use public datasets, such as the United States Department of Agriculture (USDA)'s Cropland Data Layer (CDL), as weak labels for model training [7]. Different DL architectures, such as convolutional neural networks (CNNs), deep autoencoders and recurrent neural networks with long short-term memory (LSTM), are explored for crop mapping tasks [8]–[10]. The results suggest DL approaches outperform conventional support vector machine (SVM) and tree-based models in providing semantic information on the input images.

Unfortunately, obtaining appropriate ground truth for an arbitrary region is challenging. Public datasets such as CDL are only available for a few countries and are usually released after harvest season. On the other hand, the training datasets collected by surveys can provide reliable and timely references for model training. Still, the process can be costly, labour-intensive, and sometimes unfeasible, especially in underdeveloped countries. In the absence of ground truth, existing work usually adopts the "direct transfer strategy" that trains a classifier first using available labelled data for other regions and then applies the trained model to the target region [11], [12]. However, spectral features of crops have both inter-region variability and inter-annual variability due to changes in soil composition, climate conditions, and crop progress [13]. These variability collectively contribute to the distribution shift between the training data (source domain) and the test data (target domain). Consequently, the direct transfer strategy often leads to poor performance on new and unseen regions and years as it compromises an implicit assumption of the machine learning-based crop mapping approaches: the labelled training data and the data from the target region are independent and identically distributed (i.i.d), or at least come from similar distributions.

To address this issue, various methods have been developed aiming to enhance the model's ability on unseen domains. One effective approach involves training the model by incorporating multi-year data and the respective phenological metrics as the major inputs [14]. This method helps the model to capture the temporal variations in spectral patterns for target crops caused by changing environmental and climate conditions. However, their approach only enhances the model's ability to generalise over different years of the same region, while the cross-region issue remains unsolved. Transfer learning [11], [12], [15]–[17] is a potent method that harnesses knowledge acquired from a source domain to enhance performance in

This work has been submitted to the IEEE for possible publication. Copyright may be transferred without notice, after which this version may no longer be accessible. This paper was produced by Yiqun WANG, Hui HUANG, and Radu STATE from the Services and Data Management Research Group (SEDAN), The Interdisciplinary Centre for Security, Reliability and Trust (SnT), University of Luxembourg, Luxembourg. (email: yiqun.wang@uni.lu, hui.huang@uni.lu, radu.state@uni.lu)

Yiqun WANG is the first author. Hui HUANG is the corresponding author.

a target domain. This technique involves utilizing pre-trained models and fine-tuning them on the target domain using a small amount of labelled target domain data. By doing so, the model can swiftly adapt to new data distributions and achieve improved performance. This approach works well both on cross-region and cross-year scenarios. Yet, although the amount of labelled data required by fine-tuning a pre-trained model is much smaller than training a model from scratch, collecting labels for the target domain is still labour-intensive and time-consuming.

This paper presents the Crop Generative Adversarial Network (CropGAN) to address domain shift issues that arise in early crop mapping applications, both across regions and years. We assume that only one source domain has labelled data for model training. The objective is to map a specific type of crop (e.g., corn) in a target domain for which no labelled data is available. Toward this requirement, the proposed approach considers applying an unsupervised domain adaptation technique to learn a mapping function to transform the spectral features of the target domain to the source domain while preserving their local structure. For example, the spectral features of corn cultivated in the target domain might exhibit distinct patterns from those in the source domain. After applying CropGAN, the difference between corn in the two domains should be minimized while the corn and other types of land covers in the target domain are still distinguishable. This transformation facilitates knowledge transformation from the labelled source domain to the unlabeled target domain, allowing the target domain to directly use the models trained on the source domain without degrading the performance.

From the highest level, the proposed approach consists of three key components: the pre-processor, the domain mapper, and the crop mapper. The pre-processor module employs linear interpolation to fill gaps due to cloud coverage in the Multi-Spectral Images (MSI), ensuring a complete time series. The domain mapper transforms the time-series MSI remote sensing data from the target domain to the source domain. This is achieved by utilizing an adversarial architecture [18] consisting of two generator networks and two discriminator networks. The generator learns to transform data points from the target domain to the source domain, while the discriminator distinguishes between the transformed data points and the original data points from the source domain. To train such a network, paired data that associate samples of the same category from distinct domains is required. However, the lack of labelled data within the targeted domain impedes the establishment of direct associations between datasets, presenting a barrier to forming explicit correlations between disparate domains. To overcome this obstacle, the domain mapper incorporates a cycle consistency loss [18] to ensure the transformed data points can be accurately reconstructed back into their original domain, eliminating the need for paired data. Finally, the crop mapper, which is a CNN-based model trained on the source domain, can be directly applied to the transformed data to accurately determine the cultivation locations of the specified target crop on the target domain.

Our contributions can be summarized as follows:

- Propose CropGAN to address the domain shift issue due

to the inter-region and inter-year variations in remote sensing based crop mapping. By employing unsupervised domain adaptation techniques with the integration of time-series satellite imagery, the proposed approach effectively addresses the challenges posed by limited or unavailable labelled data in target domains. This approach enables accurate crop mapping in such regions.

- Design and implement a fully functional system based on the CropGAN approach to accurately locate the specific crop of the interest in regions without labelled data.
- Conduct cross-region and cross-year experiments using datasets of regions from three countries, the USA, China, and Canada, to evaluate the proposed approach. The results demonstrate superior performance compared to the baseline method, confirming the effectiveness and accuracy of the CropGAN approach for crop mapping.

The rest of this paper is organised as follows. Section II describes related works. Section III presents the data and study areas. The methodology is described in Section IV. Experiment setup and results are presented in Section V. Finally, the discussion and conclusions are presented in Section VI.

II. RELATED WORKS

Remote sensing-based crop-type mapping has undergone significant advancements with the adoption of machine learning methods. Traditionally, techniques such as SVM and random forest (RF) have been widely utilized for crop classification using remote sensing data [19]–[21]. However, the emergence of deep learning methods has brought about a revolution in this field by leveraging their ability to automatically extract meaningful representations from data.

Deep learning models, such as LSTM networks and CNNs, have exhibited impressive performance in crop type mapping using remote sensing imagery [8], [10], [22]. They excel at capturing temporal and spatial characteristics, enabling accurate classification of various crop types. By training on labelled crop datasets, these models can learn complex relationships between spectral, spatial, and temporal features, leading to improved accuracy in distinguishing crop types. However, deep learning models encounter an adaptation problem when it comes to effectively capturing and comprehending the intricate relationships and variations in crop patterns across different regions and time periods.

To address this challenge, training the model with multi-year crop data proves to be a valuable adaptation method. Recent studies, including [14], emphasize the importance of incorporating multi-year crop data from a specific region as it enhances the model's understanding of temporal patterns, variations, and trends within that geographic context. This approach enhances the accuracy and reliability of crop classification by considering interannual climate variations and capturing the unique characteristics of the region. Leveraging region-specific multi-year data enables the model to become more robust to phenology shifts, ensuring consistent performance across different years. Training on multi-year crop data from the same region serves as an effective adaptation technique, resulting in more precise and dependable crop

mapping outcomes within a particular geographic area. A key drawback of the multi-year crop data training method is its high reliance on labelled data. To effectively train deep learning models, a large number of accurately labelled samples are needed. However, collecting such a vast amount of labelled data from diverse regions and years is a challenging task. The process is time-consuming, costly, and often impractical due to the effort and resources required.

To address this challenge, transfer learning techniques have been introduced, allowing the knowledge learned from a source domain, where labelled samples are abundant, to be transferred and applied to a target domain with limited labelled samples [11], [15].

Direct transfer [11], [12] is a commonly used transfer learning approach in remote sensing-based crop type mapping. It involves training models on regions with abundant labelled samples and directly applying them to other regions. This approach assumes that the knowledge learned from the source domain is applicable to the target domain. While direct transfer can be a simple and effective method, it may encounter difficulties due to the domain shift problem, where the characteristics of the target region, such as soil types, climate conditions, or crop varieties, differ significantly from those of the source region.

To overcome the limitations of direct transfer and address domain shift, fine-tuning has emerged as a valuable transfer learning technique. Fine-tuning involves taking a pre-trained model from the source domain and further training it using a smaller set of labelled samples from the target domain. By leveraging the knowledge already acquired from the source domain, fine-tuning enables the model to adapt and specialize for the crop classification task in the target domain [23], [24]. This adjustment of the pre-trained model's parameters allows it to capture the specific features and characteristics of the target domain, enhancing its performance in crop classification.

Fine-tuning has demonstrated promising results in improving the accuracy of crop classification models. For instance, researchers have employed pre-trained deep learning models, such as VGG16 or ResNet, which are initially trained on large-scale datasets like ImageNet, and then fine-tuned them using crop samples from the target domain [16], [17]. By transferring the knowledge acquired from a large and diverse dataset, the fine-tuned models exhibit enhanced capabilities in classifying crops accurately, even with limited labelled samples from the target domain.

Despite the effectiveness of fine-tuning, it still relies on labelled samples from the target domain, which can be a labour-intensive and time-consuming process, especially in developing or undeveloped regions. Compared with the aforementioned supervised methods, unsupervised domain adaptation (UDA) methods can transfer knowledge learned from a source domain with a large number of labelled training samples to a target domain with only unlabeled data [25]. The core idea behind UDA is to align the feature distributions between the source and target domains, ensuring that the model learns transferable representations. By achieving distribution alignment, UDA facilitates effective knowledge transfer and improves the performance of crop classification

models in the absence of labelled samples from the target domain. By aligning the feature distributions, these methods enable the model to learn domain-invariant representations, enhancing its ability to generalize from the source domain to the target domain.

Various techniques have been developed for unsupervised domain adaptation in remote sensing-based crop type mapping based on UDA. [26] introduced the deep adaptation crop classification network (DACCN) based on UDA principles for crop type mapping. Additionally, the concept of multi-source UDA (MUDA) has been explored, leveraging knowledge from multiple source domains to achieve superior results compared to single-source UDA (SUDA). [27] proposed the multi-source UDA crop classification model (MUCCM) for unsupervised crop mapping. These UDA approaches alleviate the reliance on labelled data from the target domain, making crop mapping more feasible in various settings.

In this paper, an alternative approach is proposed to address the domain shift problem in early crop mapping without relying on labelled data from the target domain. Instead of focusing on learning transferable representations like UDA, our method employs CropGAN to transform the original unlabelled data from the target domain into the source domain. By leveraging the power of CropGAN, the objective is to bridge the domain gap and enable the model to effectively utilize the labelled data from the source domain for early crop mapping in the target domain. This approach provides a practical solution for overcoming the scarcity of labelled data in the target domain, making crop mapping more feasible and accurate in diverse settings.

III. DATA AND STUDY AREAS

A. Study area

This paper chose corn as the example crop to demonstrate the cross-domain capability of the proposed approach. That is, the objective is to map corn cultivation locations in a target domain using models trained by labelled data from a source domain. The target and source domains could differ in their geographic locations (i.e., cross-region) or be in the same region in different years (i.e., cross-year). Note that, the proposed approach can be applied to other types of crops. Toward this end, the study areas include the following regions: Jackson County, Minnesota, Cavalier County, North Dakota, and Sussex County, Delaware of the USA, and two sub-areas from Jilin Province, China, and Quebec, Canada, respectively. For a visual depiction of the geographical locations of these counties and areas, please refer to Figure 1 and 2.

These counties and areas exhibit distinct environmental conditions, including variations in temperature, precipitation, evaluation, and solar radiation. The environmental condition metrics for the selected areas are shown in Table I. Moreover, the crop calendar for corn differs across these areas, as shown in Figure 3. The above differences collectively affect the development of corn in these regions. For example, figure 4a illustrates a notable disparity between the NDVI values observed in the early growth phase of corn in Jackson County between 2019 and 2020. Notably, the NDVI value curve

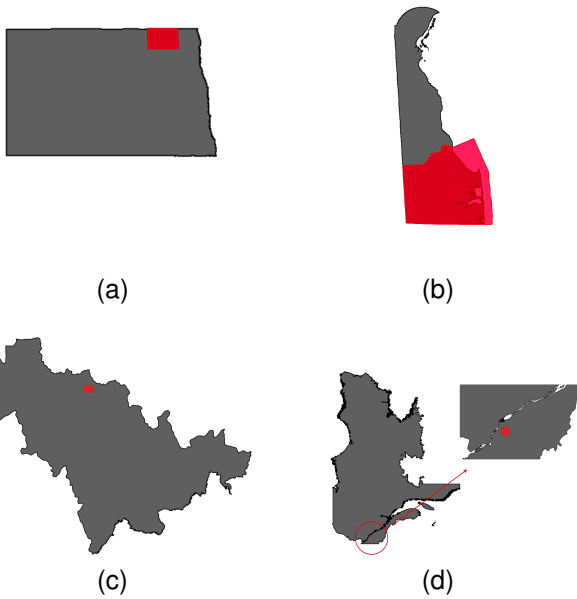


Fig. 1. The Study areas for the cross-region problem. (a) Cavalier County, North Dakota, USA. (b) Sussex County, Delaware, USA. (c) Region (from 44.97°N to 45.14°N latitude and from 125.49°W to 125.86°W longitude), Jilin Province, China. (d) Region (from 45.68°N to 45.91°N latitude and from -73.09°W to -72.73°W longitude), Quebec, Canada.

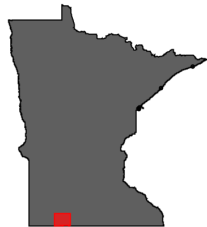


Fig. 2. The Study area for the cross-year problem. Jackson County, Minnesota, USA.

TABLE I

THE ENVIRONMENTAL CONDITIONS OF THE SOURCE DOMAIN AND THE TARGET DOMAINS. ID 1 REPRESENTS JACKSON COUNTY. ID 2 REPRESENTS THE CAVALIER COUNTY. ID 3 REPRESENTS THE STUDY AREA IN CHINA. ID 4 REPRESENTS SUSSEX COUNTY. ID 5 REPRESENTS THE STUDY AREA IN CANADA. "T" REPRESENTS THE YEARLY AVERAGE TEMPERATURE. "P" STANDS FOR THE AVERAGE HOURLY PRECIPITATION. "E" SIGNIFIES THE AVERAGE HOURLY EVAPORATION. "R" INDICATES THE SURFACE NET SOLAR RADIATION.

ID	Year	T(K)	P(mm/h)	E(mm/h)	R(kJ/m ²)
1	2019	289.02	2.60	-1.01	4688.12
1	2020	289.93	1.48	-1.11	5118.46
1	2021	290.76	1.06	-1.06	5245.53
1	2022	289.66	1.54	-1.11	4967.67
2	2019	286.24	1.04	-0.92	4996.68
3	2019	290.03	1.99	-1.99	12542.54
4	2019	294.37	1.62	-1.29	5962.68
5	2019	288.86	1.27	-1.03	5431.65

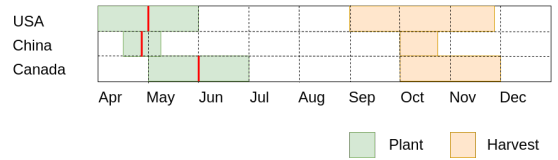


Fig. 3. The crop calendar for corn. The red lines represent the average dates of the planting periods.

exhibited an earlier increase in 2020 compared to the pattern observed in 2019. Consequently, a model trained on the data from Jackson County in 2019 can not work well in the case of 2020, as the distributions of their spectral features over time are not i.i.d.. Figure 5 complements the observation by comparing the NDVI values of corn between the study areas in the USA and those in China and Canada. In China, the maximum NDVI value is higher than that observed in the USA. Additionally, in Canada, there is a notable trend of increased NDVI values occurring approximately 30 days earlier compared to the pattern observed in the USA.

B. Reference Data

The CDL and the Canada AAFC Annual Crop Inventory are used as the ground truth for the source domains. The CDL [7], a crop-specific land cover raster map dataset available for the entire conterminous U.S. land area (CONUS) at 30 m resolution provided by the USDA, regularly provides information on the annual temporal and spatial distribution of corn, as well as the area dedicated to its cultivation. However, for the target domains, official ground reference data for China is currently unavailable. Fortunately, [6] published maps of corn and soybean with a spatial resolution of 10 meters for Northeast China from 2017 to 2019. As a result, the 2019 crop maps from [6] are regarded as the ground truth reference for the study area in China. Additionally, the Canada AAFC Annual Crop Inventory is used as the ground truth for Canada with a spatial resolution of 30 meters.

C. Remote Sensing Data

The remote sensing data in this work are MSI images captured by the Sentinel-2 satellites, which have been widely used for many agricultural applications in the community [8], [28]. Sentinel-2 provides high-resolution MSI images (up to 10m) with a revisit time of 5 days, allowing for frequent monitoring of crop growth and changes. Its wide spectral coverage, including visible, near-infrared, and shortwave infrared bands, enables accurate assessment of vegetation health, crop type identification, and mapping. In this study, 6 bands, including B2 (Blue), B3 (Green), B4 (Red), B8 (Near-Infrared), B11 (Shortwave Infrared 1) and B12 (Shortwave Infrared 2), are used to map the target crop in early seasons.

As described, our primary objective is to locate the specific crop (corn) with cross-domain problems at an earlier growth stage. As a result, the time series remote sensing data should start after the planting period and conclude before the onset of the crop harvest period. Referring to Figure 3, it can be observed that the corn harvesting season typically starts in

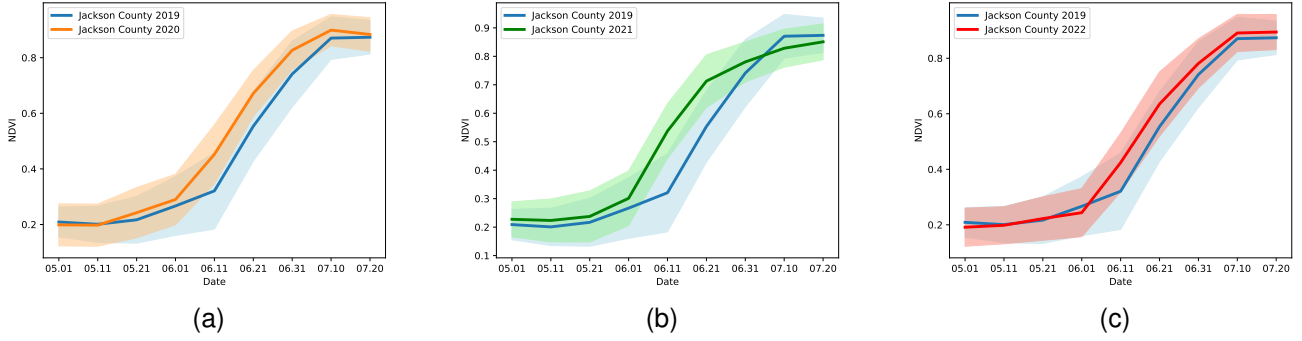


Fig. 4. The average time-series NDVI of corn for the source domain and target domains in the USA. (a) Jackson County 2019 vs. Jackson County 2020. (b) Jackson County 2019 vs. Jackson County 2021. (c) Jackson County 2019 vs. Jackson County 2022.

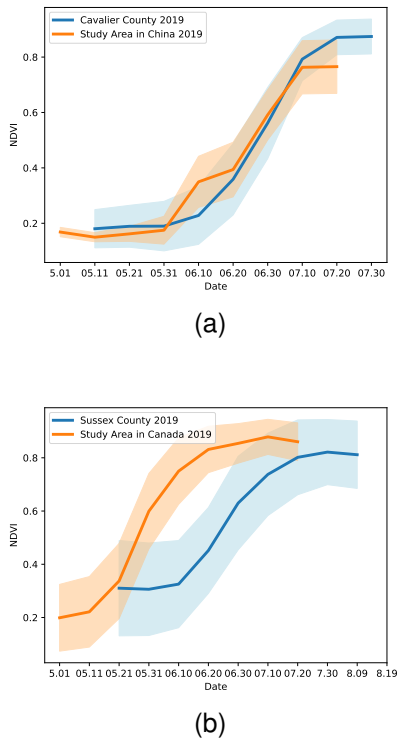


Fig. 5. The average time-series NDVI of corn for the source domain and target domains between USA, China, and Canada. (a) Cavalier County 2019 vs. Study area in China 2019. (b) Sussex County 2019 vs. Study area in Canada 2019.

early September in the USA and begins in early October in China and Canada. Planting, on the other hand, starts at the beginning of April in the USA, in mid-April in Jilin Province, China, and at the beginning of May in Québec, Canada. Furthermore, to minimize the impact of variations in the crop calendar, the beginning dates of our annual collection of remote sensing data for different countries are based on the average planting dates shown in Figure 3. For Jackson County the date spans from May 1st to July 30th, encompassing a total of nine time points with a ten-day observation window. The start date of the extracted remote sensing data from China is ten days earlier than that from the study areas in the USA. The

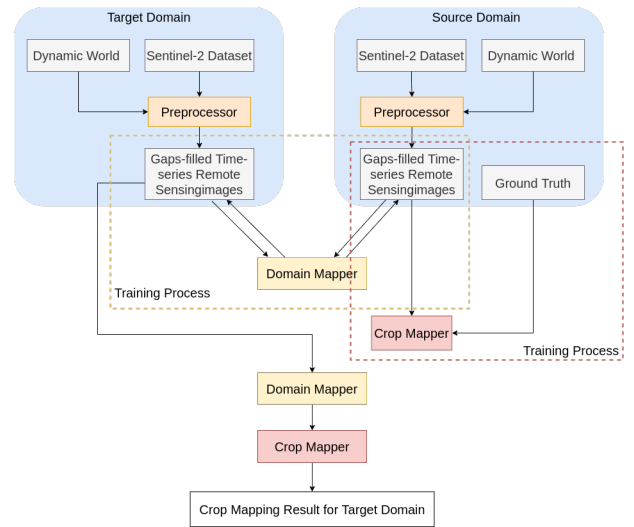


Fig. 6. The architecture of our cross-domain crop mapping system.

extracted data for China encompasses MSI images from May 1st, while for Cavalier County, USA, it starts from May 10th. Similarly, for Canada, the data involves MSI images beginning on May 30th, a 30-day later from the study area in Sussex County, USA, which started on May 1st. This approach gets the remote sensing data which covers the vegetation growth session before the crop harvesting season.

Additionally, this work employs the Dynamic World dataset [29]. It is a high-resolution 10m near-real-time (NRT) Land Use/Land Cover (LULC) dataset and features class probabilities and label data for nine distinct categories, including cropland. It is utilized to identify and select areas of cropland, enabling us to maintain a concentrated analysis solely within these regions.

IV. METHODOLOGY

A. System Overview

The system architecture of our cross-domain crop mapping method is illustrated in Figure 6. The system comprises three key components: the pre-processor, the domain mapper, and the crop mapper. The pre-processor provides the composited

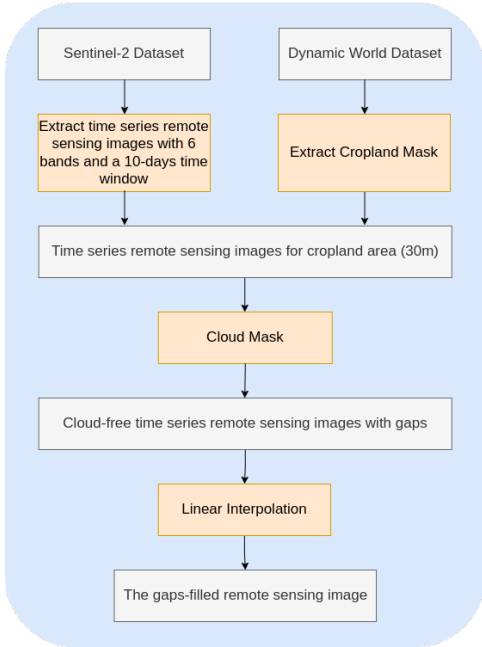


Fig. 7. The architecture of the pre-processor.

MSI images and employs a linear interpolation method to fill gaps in the images, ensuring a complete time series of remote sensing data. The domain mapper, based on the adversarial neural network, facilitates the transformation of time-series remote sensing data from the target domain to the source domain. Lastly, the crop mapper, utilizing a CNN-based model, is trained on the labelled data from the source domain. Then it receives the transformed target domain data from the domain mapper as input data to map the crop of the interest in the target domain. This comprehensive system design enables robust and precise early crop mapping within the target domain, in scenarios where labelled data is scarce or absent, addressing the challenge of domain shift.

B. Pre-processor

The pre-processor aims at providing complete time-series remote sensing data by filling gaps between MSI images due to cloud cover, atmospheric interference, or sensor limitations. The processing pipeline is outlined in Figure 7.

Initially, the pre-processor retrieves MSI images encompassing the entire specified study area. These images, sourced from the Sentinel-2 Dataset, are captured at regular intervals of 10 days as an image group. Ultimately, nine image groups are assembled, starting from the crop planting date.

Concurrently, to exclude non-agricultural lands in the MSI images, the pre-processor extracts the cropland mask during the crop growing season from the Dynamic World dataset and reprojects it into a consistent 30-meter resolution to ensure uniformity. After filtering the non-agricultural lands out using the cropland mask, the MSI images in nine image groups are specific to the agricultural lands.

Within each image group, the pre-processor employs Sentinel Hub’s cloud detector [30] to apply cloud masks on the Sentinel-2 MSI images. This process amalgamates the images,

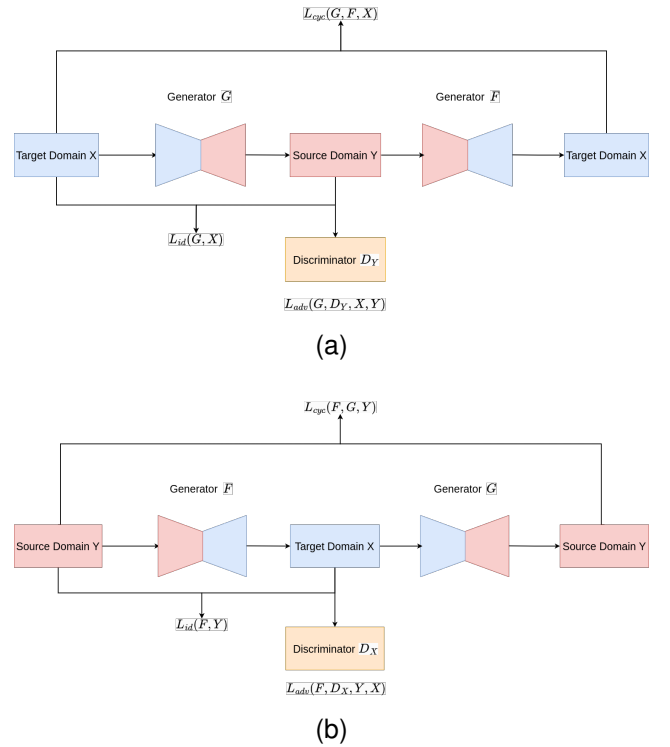


Fig. 8. The CropGAN structure.

preserving the mean values of the cloud-free MSI images. Consequently, a composite remote sensing image at a clear, 30-meter resolution is generated.

Through the pre-processor, a set of nine high-quality time-series remote sensing images is generated. These images are characterized by their absence of clouds and gaps, and they consist of six bands, all with a spatial resolution of 30 meters. These images provide a comprehensive and continuous record of the vegetation dynamics over time, enabling an in-depth analysis of temporal patterns and changes in vegetation growth.

C. Domain Mapper

The domain mapper is referred as CropGAN, which stands for Crop Generative Adversarial Network. CropGAN serves as the key component in our framework for transforming time-series remote sensing data points between different domains. As shown in Figure 8, the domain mapper consists of two generator networks, G and F , and two discriminator networks, D_X and D_Y . The visual representations of the generator and discriminator structures can be observed in Table II and Table III, respectively. Given two crop mapping domains X and Y , $\{x_i\}_{i=1}^N$ is the time-series remote sensing data in Domain X , and $\{y_j\}_{j=1}^M$ is the time-series remote sensing data in Domain Y . CropGAN is trained to learn the mappings between different data distributions from different domains: $G : X \rightarrow Y$ and $F : Y \rightarrow X$. In the training process, the generators and discriminators play distinct roles. The generator’s primary task is to transform the data from one domain to another, while the discriminator’s main objective is to differentiate between real and transformed data. As the training progresses, both

TABLE II

THE GENERATOR STRUCTURE. EACH ENCODER LAYER CONSISTS OF AN INSTANCE NORMALIZATION LAYER, AN ACTIVATION LAYER AND A POOLING LAYER. EACH DECODER LAYER CONSISTS OF AN INSTANCE NORMALIZATION LAYER, AN ACTIVATION LAYER AND AN UPSAMPLING LAYER.

Layer	Input Shape	Output Shape	Activation
Input	9x6x1	9x6x1	-
Encoder 1	9x6x1	7x5x4	LeakyReLU
Encoder 2	7x5x4	5x4x8	LeakyReLU
Encoder 3	5x4x8	3x3x16	LeakyReLU
Encoder 4	3x3x16	1x2x32	LeakyReLU
Decoder 4	1x2x32	3x3x16	LeakyReLU
Decoder 3	3x3x16	5x4x8	LeakyReLU
Decoder 2	5x4x8	7x5x4	LeakyReLU
Decoder 1	7x5x4	9x6x2	LeakyReLU
Decoder 1	7x5x2	9x6x1	LeakyReLU
Output	9x2x1	9x2x1	ReLU

TABLE III

THE DISCRIMINATOR STRUCTURE. IN REPRESENTS AN INSTANCE NORMALIZATION LAYER.

Layer	Input Shape	Output Shape	Activation
Input	9x6x1	9x6x1	-
Conv 1	9x6x1	9x6x4	LeakyReLU
IN 1	9x6x4	9x6x4	-
Conv 2	9x6x4	4x3x8	LeakyReLU
IN 2	4x3x8	4x3x8	-
Conv 3	4x3x8	2x1x16	LeakyReLU
IN 3	2x1x16	2x1x16	-
Conv 4	2x1x16	1x1x1	LeakyReLU
Ouput	1x1x1	1	ReLU

networks improve iteratively until an equilibrium is reached where the generator generates highly realistic data and the discriminator cannot reliably distinguish between real and fake samples. For example, when the discriminator D_Y can not distinguish whether the data generated by the generator G is from source domain Y or not, it means that the generator G has been well-trained.

To ensure the creation of effective generators, the objectives for both generators and discriminators are established as follows:

Adversarial Loss: This loss function is inspired by generative adversarial networks (GANs) and encourages the generator to produce transformed data from one domain that is indistinguishable from real data in the other domain. It is computed by the discriminator network, which aims to classify the generated data as fake while the generator aims to fool the discriminator by generating realistic data.

$$\mathcal{L}_{adv}(G, D_Y, X, Y) = \mathbb{E}_{y \sim p_{data}(y)} [\log D_Y(y)] + \mathbb{E}_{x \sim p_{data}(x)} [1 - \log D_Y(G(x))] \quad (1)$$

$$\mathcal{L}_{adv}(F, D_X, Y, X) = \mathbb{E}_{x \sim p_{data}(x)} [\log D_X(x)] + \mathbb{E}_{y \sim p_{data}(y)} [1 - \log D_X(F(y))] \quad (2)$$

Cycle Consistency Loss: The cycle consistency loss ensures that the mapping from the source domain to the target domain and back to the source domain is consistent. It measures the difference between the original input data and the data reconstructed after going through both generator mappings.

Through the minimization of this loss, the preservation of crucial features during the transformation process is enforced.

$$\mathcal{L}_{cyc}(G, F, X) = \mathbb{E}_{x \sim p_{data}(x)} [\|x - F(G(x))\|_1] \quad (3)$$

$$\mathcal{L}_{cyc}(F, G, Y) = \mathbb{E}_{y \sim p_{data}(y)} [\|y - G(F(y))\|_1] \quad (4)$$

Identity Loss: The identity loss encourages the generator to preserve the identity of the input data. It computes the difference between the generator output and the input data. The objective of minimizing this loss is to ensure that the generator does not make unnecessary alterations to the data and maintains its essential characteristics.

$$\mathcal{L}_{id}(G, X) = \mathbb{E}_{x \sim p_{data}(x)} [\|G(x) - x\|_1] \quad (5)$$

$$\mathcal{L}_{id}(F, Y) = \mathbb{E}_{y \sim p_{data}(y)} [\|F(y) - y\|_1] \quad (6)$$

Total Loss: The total loss is a combination of these losses, weighted by respective coefficients, and aims to optimize the generators and discriminators simultaneously to achieve high-quality time-series NDVI and EVI data transformation while maintaining consistency and identity preservation.

$$\mathcal{L}_{total} = \alpha(\mathcal{L}_{adv}(G, D_Y, X, Y) + \mathcal{L}_{adv}(F, D_X, Y, X)) + \beta(\mathcal{L}_{cyc}(G, F, X) + \mathcal{L}_{cyc}(F, G, Y)) + \sigma(\mathcal{L}_{id}(G, X) + \mathcal{L}_{id}(F, Y)) \quad (7)$$

Training stop criteria based on the Total Loss: In the evaluation of CycleGAN, it is common practice to assess the model's performance on paired datasets, even though the model is trained without explicitly using paired data. However, in the case of CropGAN, there are no paired datasets available for evaluation due to the lack of labelled data in the target domain. This poses a challenge in evaluating the model's performance using traditional paired dataset evaluation metrics.

To overcome this limitation, the total loss is employed as an evaluation metric. After the CropGAN network has reached a stable state for the training process after several training epochs, the model is selected associated with the smallest total loss. This particular model is then designated as our well-trained model.

This approach allows us to tackle the absence of paired datasets for evaluation in CropGAN and obtain an objective measure of the model's performance.

D. Crop Mapper

The crop mapper utilizes a Convolutional Neural Network (CNN) as the core component for crop classification. The CNN architecture consists of convolutional, pooling, and fully connected layers, designed to learn hierarchical representations of the input data and capture both low-level features and high-level semantic information. However, due to the small structure of the time-series remote sensing input data, pooling layers are omitted. The crop mapper structure is shown in Table IV.

A single CNN model is trained exclusively on the source domain data to optimize its performance for the specific

TABLE IV
THE CROP MAPPER STRUCTURE. BN REPRESENTS A BATCH NORMALIZATION LAYER. CONV REPRESENTS A CONVOLUTIONAL LAYER. FC REPRESENTS A FULLY CONNECTED LAYER.

Layer	Input Shape	Output Shape	Activation
Input	9x6x1	9x6x1	-
Conv 1	9x6x1	9x6x2	ReLU
BN 1	9x6x2	9x6x2	-
Conv 2	9x6x2	4x3x2	ReLU
BN 2	4x3x2	4x3x2	-
Conv 3	4x3x2	2x1x4	ReLU
BN 3	2x1x4	2x1x4	-
Flatten	2x1x4	8	-
FC 1	8	4	ReLU
FC 2	4	1	ReLU
Output	1	1	Softmax

characteristics and patterns of the source domain. As explained above, directly applying this trained model to the target domain can result in suboptimal performance due to domain shift, where the target domain data exhibits different distributions and variations compared to the source domain data. Therefore, before applying the trained crop mapper on a given target domain, the remote sensing data of the target domain should be first transformed using the domain mapper to resemble those of the source domain. Subsequently, to derive the crop mapping result, the transformed data is fed into the crop mapper.

By combining the domain mapper and the crop mapper, our methodology achieves robust and accurate crop mapping results even in the presence of domain shift. This approach leverages the strengths of both models to effectively tackle the challenges posed by different domains in crop mapping applications.

V. EXPERIMENT SETUP AND RESULTS

A. Experiment setup

This work designs two sets of experiments to comprehensively evaluate the cross-domain performance of the proposed CropGAN method. The first set of experiments investigates the cross-year scenario, where Jackson County from 2020 to 2022 is considered the target domain, and Jackson County in 2019 serves as the foundational source domain. In contrast, the second set of experiments focuses on the cross-region scenario, where Cavalier County 2019 and Sussex County 2019 serve as the source domains, respectively. The target domains include the sub-areas from Jilin Province, China, and Quebec, Canada.

In each experiment, the crop mapper is trained by using 70% of randomly selected labelled data from the source domain. The remaining 30% is divided equally into validation and test dataset. To train the CropGAN model, the unlabelled remote sensing data from the target domain is combined with the labelled data from the source domain. During training, the number of epochs is set to 300, and a batch size of 64 is used. For optimization, the Adaptive Moment Estimation (Adam) optimizer is employed with a learning rate of 0.005 and an exponential decay rate of 0.5 for the first moment estimates. It's worth noting that the coefficients of the total loss function in the experiments are set to 1, 10, and 5.

The results are compared with the direct transfer method as the baseline method, which involves directly applying the trained crop mapper to the target domains without any refinement or preprocessing steps. This comparison enabled us to showcase the effectiveness and improvements achieved by our proposed approach.

B. Evaluation Metrics

To assess the performance of the binary corn crop mapping, the following metrics are used:

The Kappa coefficient: measures the agreement between the predicted and observed classifications, taking into account the agreement that would occur by chance alone.

Overall Accuracy (OA): represents the proportion of all correctly classified items to the total number of items in the dataset.

F1 Score: is a single metric that combines precision and recall to provide an overall measure of a model's accuracy in classification tasks. It balances the trade-off between correctly identifying positive instances and minimizing false positives and false negatives.

C. Results

During the training process of CropGAN, a comprehensive evaluation approach is utilized to assess the model's performance and select the well-trained model.

At the end of each training epoch of CropGAN, data is transformed from the target domain to the source domain. This transformed data is then classified using the crop mapper, and three evaluation metrics, namely the OA, F1 score, and Kappa coefficient, are calculated based on the ground truth.

In addition to the evaluation metrics, we also calculate the total loss between the transformed data and the source domain data to assess how well the CropGAN model aligns the target domain data with the source domain data.

To select the well-trained CropGAN model, the model with the lowest total loss value is chosen. This indicates that the model has successfully minimized the domain shift and effectively transformed the target domain data to resemble the source domain data. The best-trained CropGAN models for the USA target domains (specifically, Jackson County from 2020 to 2022) correspond to epochs 178, 252, and 117. Similarly, the most proficiently trained CropGAN models for the study areas in China and Canada are linked to epochs 238 and 148.

By incorporating both the evaluation metrics and the total loss calculation, our evaluation approach ensures that the selected CropGAN model not only achieves high accuracy in crop mapping but also effectively mitigates the domain shift problem.

Additionally, experiments are carried out to compare the performance of the direct transfer method and our proposed CropGAN method in crop mapping. For the direct transfer method, the target domain data is directly fed into the crop mapper to provide the crop mapping result. Following this, 3 metrics are calculated as well. The results of the cross-year and cross-region experiments are presented in Table V and

TABLE V
THE METRICS COMPARISON OF CROSS-YEAR EXPERIMENTS. BETTER METRICS ARE INDICATED IN BOLD.

Source Domain	Target Domain	CropGAN			Baseline		
		OA	F1	Kappa	OA	F1	Kappa
2019 Jackson	2020 Jackson	0.8149	0.8153	0.6310	0.6162	0.4304	0.2623
2019 Jackson	2021 Jackson	0.8440	0.8347	0.6903	0.5789	0.3249	0.1868
2019 Jackson	2022 Jackson	0.8902	0.8992	0.7792	0.6491	0.4871	0.3141

TABLE VI
THE METRICS COMPARISON OF CROSS-REGION EXPERIMENTS. "SA" REPRESENTS THE "STUDY AREA". BETTER METRICS ARE INDICATED IN BOLD.

Source Domain	Target Domain	CropGAN			Baseline		
		OA	F1	Kappa	OA	F1	Kappa
2019 Cavalier	2019 SA (China)	0.7155	0.7088	0.4308	0.6268	0.5232	0.2435
2019 Sussex	2019 SA (Canada)	0.7647	0.8174	0.4916	0.7076	0.6861	0.4501

VI. The tables provide a comprehensive comparison of various evaluation metrics.

Overall, the CropGAN method consistently outperformed the direct transfer method in terms of 3 metrics. These results highlight the effectiveness of our proposed approach in improving the accuracy of early crop mapping.

In Jackson County in 2020, the CropGAN method achieved a higher OA of 0.8149 compared to the direct transfer method's OA of 0.6162. Similarly, the CropGAN method exhibited a higher Kappa coefficient value of 0.6310, surpassing the direct transfer method's Kappa coefficient of 0.2623. The F1 score also showed improvements with the CropGAN method, reaching 0.8153 from 0.4304. For Jackson County in 2021, the CropGAN method outperformed the direct transfer method across all metrics. Notably, the CropGAN method achieved a significantly higher Kappa coefficient of 0.6903 compared to the direct transfer method's Kappa coefficient of 0.1868. The OA and F1 score also exhibited notable improvements with our proposed approach. In Jackson County in 2022, the CropGAN method outperformed the direct transfer method, reaching a 0.7792 Kappa coefficient compared to 0.3141. Figures 9, 10, and 11 illustrate the visualization of results for the cross-year experiments obtained using both our method and the direct transfer method. In the visualization of mapping results, green pixels represent the identified corn regions, while white pixels represent the non-corn regions. For the error images red highlights the misclassified pixels, while white represents the correctly classified pixels.

Moving on to the study area in China, our proposed CropGAN method consistently outperformed the direct transfer method. The improvement is significant, with the CropGAN method achieving an OA of 0.7155 compared to the direct transfer method's OA of 0.6268. The F1 score and Kappa coefficient also showed remarkable increases with our proposed approach from 0.5232 and 0.2435 to 0.7088 and 0.4308. In the Canadian study area, our proposed CropGAN method consistently outperformed the direct transfer method, with a notable enhancement in the F1 score, which increased from 0.6861 to 0.8174. Figures 12 and 13 illustrate the visualization of results for the cross-domain experiments obtained using both our method and the direct transfer method.

The experimental results demonstrate the superiority of the CropGAN method over the direct transfer method, showcasing

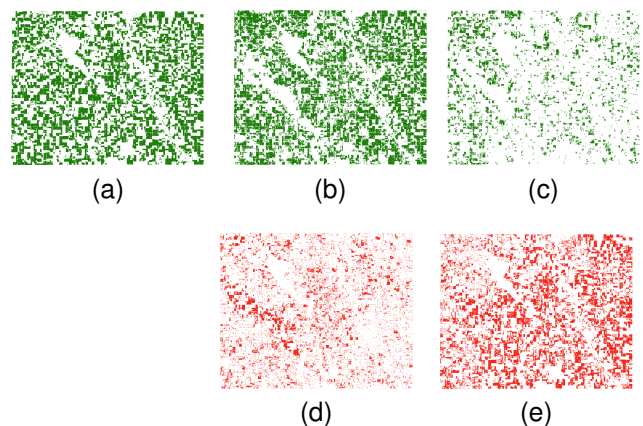


Fig. 9. Corn Crop Mapping Results Comparison for the Jackson County 2020: Our Method vs. Direct Transfer. (a) displays the ground truth. The crop mapping results are depicted in (b) for CropGAN, and (c) for the baseline method. In this visualization, green denotes corn, and white represents other crops. The corresponding error images are illustrated in panels (d) and (e) for CropGAN and the baseline method, respectively. Red highlights the misclassified pixels, and white represents correctly classified pixels.

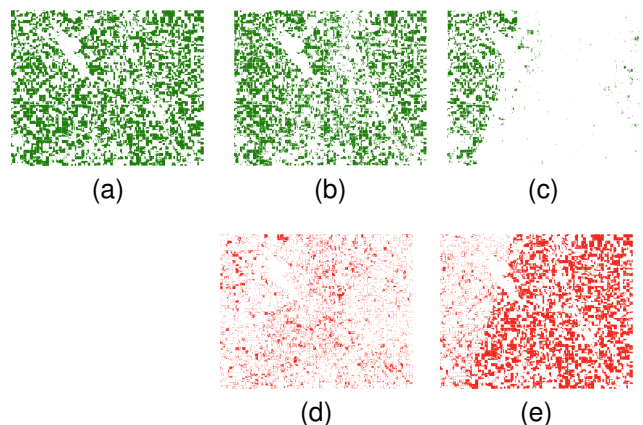


Fig. 10. Corn Crop Mapping Results Comparison for the Jackson County 2021: Our Method vs. Direct Transfer.

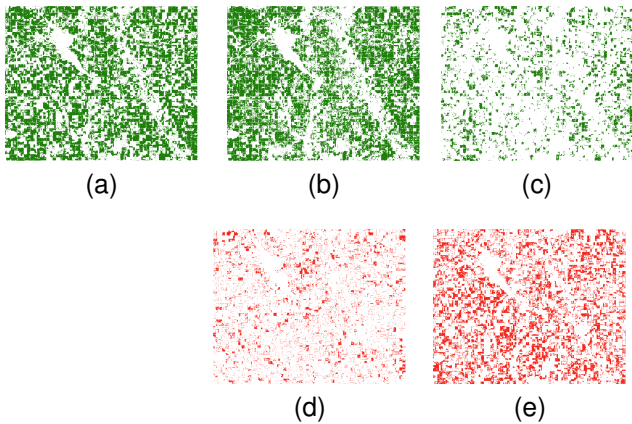


Fig. 11. Corn Crop Mapping Results Comparison for the Jackson County 2022: Our Method vs. Direct Transfer.

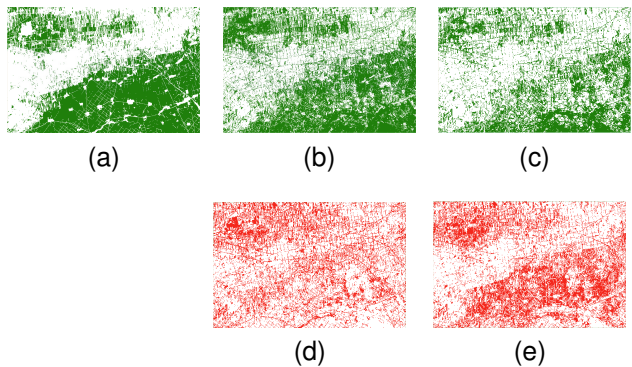


Fig. 12. Corn Crop Mapping Results Comparison for the Study Area in China: Our Method vs. Direct Transfer.

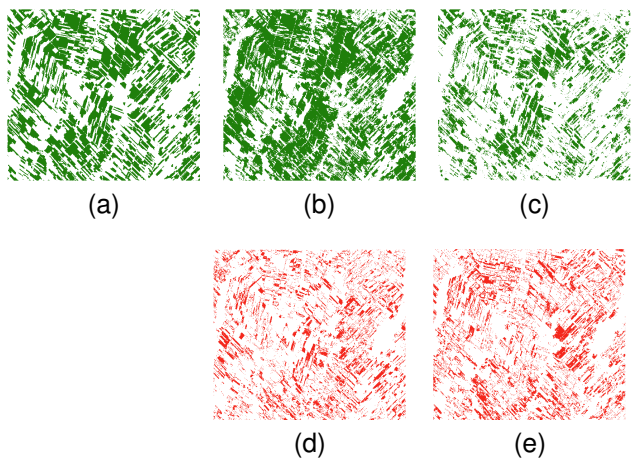


Fig. 13. Corn Crop Mapping Results Comparison for the Study Area in Canada: Our Method vs. Direct Transfer.

significant improvements in OA, F1 score, and Kappa coefficient. By leveraging the combination of labelled data from the source domain and unlabeled data from the target domains, our proposed approach effectively enhances early crop mapping accuracy.

In conclusion, the experimental results validate the effectiveness of our proposed CropGAN method in improving

crop mapping accuracy by effectively addressing cross-domain challenges. The consistent outperformance of the CropGAN method compared to the direct transfer method across various metrics highlights its potential for practical applications in the agricultural industry.

D. The t-SNE Visualization

To assess the effectiveness of our method in addressing the domain shift problem, we utilize t-distributed stochastic neighbour embedding (t-SNE) [31] visualization to analyze the distribution of corn and non-corn data in the target, transformed target, and source domains. By using t-SNE, the data points are projected into a two-dimensional space while preserving their local relationships. Figure 14 and 15 show the t-SNE visualization that illustrates the distribution of corn data points for the cross-domain experiments.

In the visualization, the orange points represent remote sensing data points of corn cropland sourced from the target domain, offering a glimpse into the data distribution within that domain. The green points denote the transformed corn cropland remote sensing data points from the target domain to the source domain, employing our proposed method. Finally, the blue points indicate the original corn cropland remote sensing data points extracted from the source domain.

Upon analyzing the t-SNE visualization, it is evident that the distribution of corn cropland remote sensing data points between the source and target domains differs. This disparity highlights the presence of a domain shift, which poses challenges for accurate crop mapping under the target domains.

However, the application of our CropGAN method resulted in an improvement in the similarity between the data distribution of the transformed target domain data (green points) and the source domain data (blue points), compared to the similarity between the original target domain data (orange points) and the source domain data (blue points). This resemblance enables the crop mapper, trained on the source domain, to effectively process the transformed remote sensing data obtained from the target domain. It coincides with our excellent crop mapping results for these years and this county.

Overall, the t-SNE visualization provides valuable insights into the effectiveness of our method in addressing the domain shift problem and highlights the impact of domain similarity on the performance of crop mapping. Through the utilization of our CropGAN method to bridge the gap between the target and source domains, we attain improved similarity in the distribution between transformed target domain data and source domain data, leading to enhanced early crop mapping accuracy.

VI. DISCUSSION AND CONCLUSIONS

Our study focuses on early crop mapping using a combination of deep learning techniques and domain adaptation. In this paper, a novel approach is introduced that harnesses the capabilities of a CycleGAN-based model, known as CropGAN, to tackle the domain shift problem between source and target domains. By transforming the remote sensing data of the target

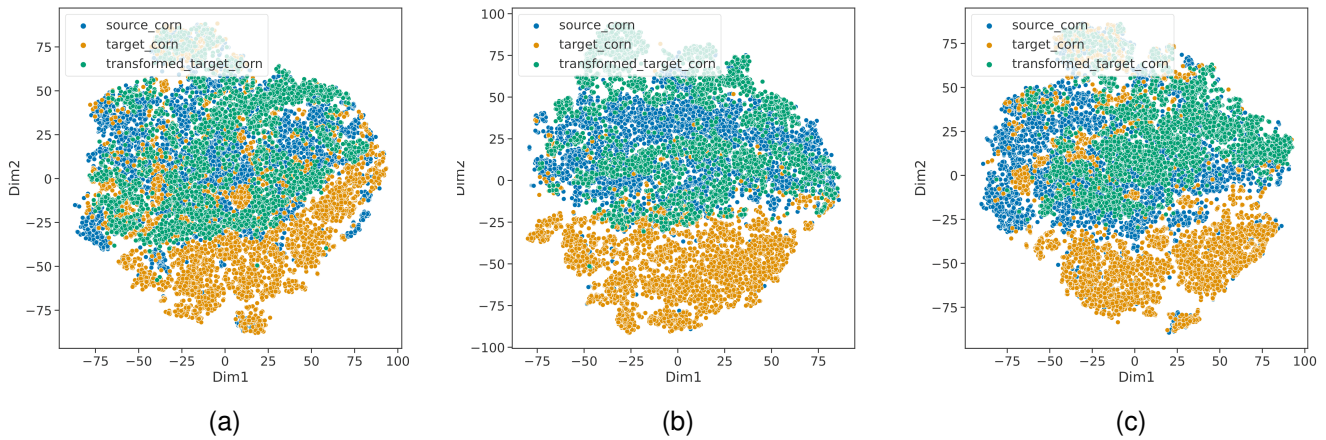


Fig. 14. The t-SNE Visualization of Corn Data Points for the Cross-Year Experiments: Comparison between Target, Transformed Target, and Source Domains. (a) Jackson County 2020. (b) Jackson County 2021. (c) Jackson County 2022.

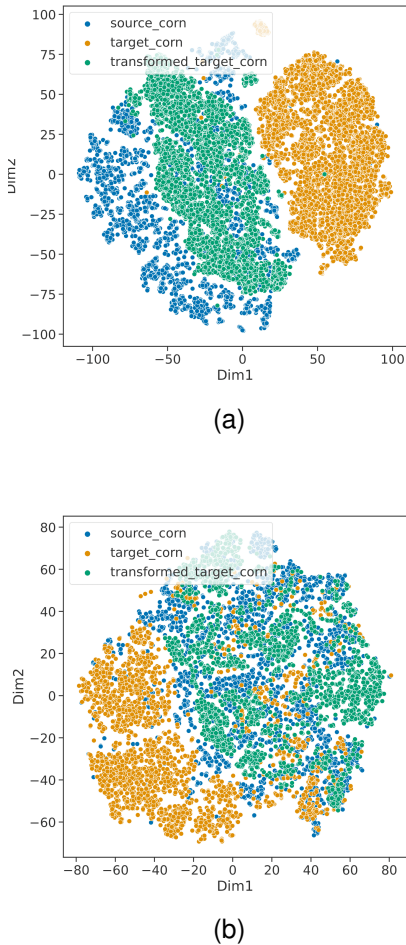


Fig. 15. The t-SNE Visualization of Corn Data Points for the Cross-Region Experiments: Comparison between Target, Transformed Target, and Source Domains. (a) The Study Area in China 2019. (b) The Study Area in Canada 2019.

domain to resemble the source domain, accurate early crop mapping outcomes are achieved.

The experimental results demonstrate the effectiveness of our approach. The performance of our method is compared with a direct transfer method, where the crop mapper is directly applied to the target domain without any preprocessing or refinement. Our method consistently outperformed the direct transfer method across multiple evaluation metrics, including the OA, F1 score, and Kappa coefficient. This indicates that the CropGAN-based domain adaptation significantly improves the accuracy of the early crop mapping in the target domain.

Additionally, the t-SNE visualization results offered insights into the distribution of corn and non-corn data in both the source and target domains. A clear distinction difference between the distributions of the two domains is observed, highlighting the domain shift challenge. However, the distribution of the transformed target domain data by CropGAN closely resembled that of the source domain, signifying the effectiveness of our method in addressing the domain shift problem.

However, it is important to acknowledge the limitations of our work. One limitation of our CropGAN work is the underlying assumption that the primary crops in the target domain and the source domain are consistent. This assumption, which implies uniformity in the dominant crop types, may not always hold true in practice, particularly when considering diverse agricultural practices across different regions. In future research, addressing this limitation and developing methods that can accommodate variations in primary crop types across domains will be a valuable direction for enhancing the robustness and applicability of our approach.

Overall, our work presents a robust and effective approach to crop mapping by combining deep learning techniques, domain adaptation using CropGAN, and rigorous evaluation metrics. The results demonstrate the superiority of our method compared to direct transfer approaches. This work contributes to the field of crop mapping by addressing the challenges of domain shift and improving the accuracy of crop classification in target domains.

REFERENCES

- [1] F. Waldner, S. Fritz, A. Di Gregorio, and P. Defourny, "Mapping priorities to focus cropland mapping activities: Fitness assessment of existing global, regional and national cropland maps," *Remote Sensing*, vol. 7, no. 6, pp. 7959–7986, 2015.
- [2] C. Singha and K. C. Swain, "Land suitability evaluation criteria for agricultural crop selection: A review," *Agricultural reviews*, vol. 37, no. 2, pp. 125–132, 2016.
- [3] J. Xue, B. Su *et al.*, "Significant remote sensing vegetation indices: A review of developments and applications," *Journal of sensors*, vol. 2017, 2017.
- [4] A. Joshi, B. Pradhan, S. Gite, and S. Chakraborty, "Remote-sensing data and deep-learning techniques in crop mapping and yield prediction: A systematic review," *Remote Sensing*, vol. 15, no. 8, p. 2014, 2023.
- [5] L. Zhang, Z. Liu, D. Liu, Q. Xiong, N. Yang, T. Ren, C. Zhang, X. Zhang, and S. Li, "Crop mapping based on historical samples and new training samples generation in heilongjiang province, china," *Sustainability*, vol. 11, no. 18, p. 5052, 2019.
- [6] N. You, J. Dong, J. Huang, G. Du, G. Zhang, Y. He, T. Yang, Y. Di, and X. Xiao, "The 10-m crop type maps in northeast china during 2017–2019," *Scientific data*, vol. 8, no. 1, p. 41, 2021.
- [7] C. Boryan, Z. Yang, R. Mueller, and M. Craig, "Monitoring us agriculture: the us department of agriculture, national agricultural statistics service, cropland data layer program," *Geocarto International*, vol. 26, no. 5, pp. 341–358, 2011.
- [8] Y. Wang, Z. Zhang, L. Feng, Y. Ma, and Q. Du, "A new attention-based cnn approach for crop mapping using time series sentinel-2 images," *Computers and electronics in agriculture*, vol. 184, p. 106090, 2021.
- [9] M. Hamidi, A. Safari, and S. Homayouni, "An auto-encoder based classifier for crop mapping from multitemporal multispectral imagery," *International Journal of Remote Sensing*, vol. 42, no. 3, pp. 986–1016, 2021.
- [10] H. Crisóstomo de Castro Filho, O. Abílio de Carvalho Júnior, O. L. Ferreira de Carvalho, P. Pozzobon de Bem, R. dos Santos de Moura, A. Olino de Albuquerque, C. Rosa Silva, P. H. Guimarães Ferreira, R. Fontes Guimarães, and R. A. Trancoso Gomes, "Rice crop detection using lstm, bi-lstm, and machine learning models from sentinel-1 time series," *Remote Sensing*, vol. 12, no. 16, p. 2655, 2020.
- [11] P. Hao, L. Di, C. Zhang, and L. Guo, "Transfer learning for crop classification with cropland data layer data (cdl) as training samples," *Science of The Total Environment*, vol. 733, p. 138869, 2020.
- [12] S. Ge, J. Zhang, Y. Pan, Z. Yang, and S. Zhu, "Transferable deep learning model based on the phenological matching principle for mapping crop extent," *International Journal of Applied Earth Observation and Geoinformation*, vol. 102, p. 102451, 2021.
- [13] V. S. Konduri, J. Kumar, W. W. Hargrove, F. M. Hoffman, and A. R. Ganguly, "Mapping crops within the growing season across the united states," *Remote Sensing of Environment*, vol. 251, p. 112048, 2020.
- [14] L. Zhong, P. Gong, and G. S. Biging, "Efficient corn and soybean mapping with temporal extendability: A multi-year experiment using landsat imagery," *Remote Sensing of Environment*, vol. 140, pp. 1–13, 2014.
- [15] A. Nowakowski, J. Mrzigił, D. Spiller, R. Bonifacio, I. Ferrari, P. P. Mathieu, M. Garcia-Herranz, and D.-H. Kim, "Crop type mapping by using transfer learning," *International Journal of Applied Earth Observation and Geoinformation*, vol. 98, p. 102313, 2021.
- [16] R. Chew, J. Rineer, R. Beach, M. O'Neil, N. Ujeneza, D. Lapidus, T. Miano, M. Hegarty-Craver, J. Polly, and D. S. Temple, "Deep neural networks and transfer learning for food crop identification in uav images," *Drones*, vol. 4, no. 1, p. 7, 2020.
- [17] I. Kalita, G. P. Singh, and M. Roy, "Crop classification using aerial images by analyzing an ensemble of dcnn's under multi-filter & multi-scale framework," *Multimedia Tools and Applications*, vol. 82, no. 12, pp. 18409–18433, 2023.
- [18] J. Zhu, T. Park, P. Isola, and A. A. Efros, "Unpaired image-to-image translation using cycle-consistent adversarial networks," in *Proceedings of the IEEE international conference on computer vision*, 2017, pp. 2223–2232.
- [19] B. Zheng, S. W. Myint, P. S. Thenkabail, and R. M. Aggarwal, "A support vector machine to identify irrigated crop types using time-series landsat ndvi data," *International Journal of Applied Earth Observation and Geoinformation*, vol. 34, pp. 103–112, 2015.
- [20] P. Hao, Y. Zhan, L. Wang, Z. Niu, and M. Shakir, "Feature selection of time series modis data for early crop classification using random forest: A case study in kansas, usa," *Remote Sensing*, vol. 7, no. 5, pp. 5347–5369, 2015.
- [21] R. Saini and S. K. Ghosh, "Crop classification on single date sentinel-2 imagery using random forest and support vector machine," *The International Archives of the Photogrammetry, Remote Sensing and Spatial Information Sciences*, vol. 42, pp. 683–688, 2018.
- [22] Z. Sun, L. Di, and H. Fang, "Using long short-term memory recurrent neural network in land cover classification on landsat and cropland data layer time series," *International journal of remote sensing*, vol. 40, no. 2, pp. 593–614, 2019.
- [23] E. C. Tetila, B. B. Machado, G. Astolfi, N. A. de Souza Belete, W. P. Amorim, A. R. Roel, and H. Pistori, "Detection and classification of soybean pests using deep learning with uav images," *Computers and Electronics in Agriculture*, vol. 179, p. 105836, 2020.
- [24] M. Lavreniuk, N. Kussul, and A. Novikov, "Deep learning crop classification approach based on sparse coding of time series of satellite data," in *IGARSS 2018-2018 IEEE International Geoscience and Remote Sensing Symposium*. IEEE, 2018, pp. 4812–4815.
- [25] Y. Ganin, E. Ustinova, H. Ajakan, P. Germain, H. Larochelle, F. Laviolette, M. Marchand, and V. Lempitsky, "Domain-adversarial training of neural networks," *The journal of machine learning research*, vol. 17, no. 1, pp. 2096–2030, 2016.
- [26] Y. Wang, L. Feng, Z. Zhang, and F. Tian, "An unsupervised domain adaptation deep learning method for spatial and temporal transferable crop type mapping using sentinel-2 imagery," *ISPRS Journal of Photogrammetry and Remote Sensing*, vol. 199, pp. 102–117, 2023.
- [27] Y. Wang, L. Feng, W. Sun, Z. Zhang, H. Zhang, G. Yang, and X. Meng, "Exploring the potential of multi-source unsupervised domain adaptation in crop mapping using sentinel-2 images," *GIScience & Remote Sensing*, vol. 59, no. 1, pp. 2247–2265, 2022.
- [28] L. Blickensdörfer, M. Schwieder, D. Pflugmacher, C. Nendel, S. Erasmi, and P. Hostert, "Mapping of crop types and crop sequences with combined time series of sentinel-1, sentinel-2 and landsat 8 data for germany," *Remote sensing of environment*, vol. 269, p. 112831, 2022.
- [29] C. F. Brown, S. P. Brumby, B. Guzder-Williams, T. Birch, S. B. Hyde, J. Mazzariello, W. Czerwinski, V. J. Pasquarella, R. Haertel, S. Ilyushchenko *et al.*, "Dynamic world, near real-time global 10 m land use land cover mapping," *Scientific Data*, vol. 9, no. 1, p. 251, 2022.
- [30] S. Skakun, J. Wevers, C. Brockmann, G. Doxani, M. Aleksandrov, M. Batič, D. Frantz, F. Gascon, L. Gómez-Chova, O. Hagolle *et al.*, "Cloud mask intercomparison exercise (cmix): An evaluation of cloud masking algorithms for landsat 8 and sentinel-2," *Remote Sensing of Environment*, vol. 274, p. 112990, 2022.
- [31] L. Van der Maaten and G. Hinton, "Visualizing data using t-sne." *Journal of machine learning research*, vol. 9, no. 11, 2008.



Yiqun WANG received the M.Sc. degree from the Karlsruhe Institute of Technology, Karlsruhe, Germany, in 2020. He is currently a Ph.D. Candidate with the Interdisciplinary Centre on Security Reliability and Trust, University of Luxembourg, Luxembourg City, Luxembourg. His research interests are in remote sensing, computer vision, and deep learning.



Hui Huang received the M.Sc. degree in computing science from the University of Glasgow, Glasgow, U.K., in 2013, and the Ph.D. degree from the University of New South Wales, Sydney, NSW, Australia, in 2018. He is currently a Research Associate with the Interdisciplinary Centre on Security Reliability and Trust, University of Luxembourg, Luxembourg City, Luxembourg. His research interests include V2X communications, autonomous driving, and intelligent transportation systems.



Radu STATE received the M.Sc. degree from the Johns Hopkins University, Baltimore, MD, USA, and the Ph.D. degree and a HDR from the University of Lorraine, Nancy, France. He is a Professor with the Interdisciplinary Center on Security and Trust in Luxembourg. He was a Professor at the University of Lorraine and a Senior Researcher at INRIA Nancy, Grand Est. Having authored more than 100 papers, his research interests cover network and system security and management.